International Journal of Science and Research (IJSR)
ISSN: 2319-7064
ResearchGate Impact Factor (2018): 0.28 | SJIF (2019): 7.583

NDVI and Land Surface Temperature Spatio-Temporal Relationship: Al Taif, Saudi Arabia, as a Case Study

Rasha Alomairi[1], Sarra Ouerghi[1, 2]

[1]Department of Geography and GIS, Faculty of Arts & Humanities, King Abdulaziz University, Jeddah, Saudi Arabia

[2]Laboratoire 3E « Eau-Energie-Environnement » (LRAD-10-02), Ecole Nationale d'Ingénieurs de Sfax, Tunisie
Email: *sarahouerghi[at]gmail.com*

Abstract: ***A key factor in different research fields, environmental and global change studies being two examples, is land surface temperature (LST). Earth - atmosphere interaction is the key parameter of the physics processes of the earth. LANDSAT 8 and LANDSAT 5 from LANDSAT series, have resulted in a great number of possibilities to investigate land processes with the use of remote sensing. This piece of research attempts to estimate LST over Al Taif city, Saudi Arabia, using LANDSAT Thermal Infrared Sensor data as a response to lack of meteorological station (one meteorological station in Al Taif). Variability of retrieved LST has been studied in terms of values of Normalized Difference Vegetation Index (NDVI) for a multiplicity of types of land cover, and in accordance with the Landsat visible and NIR channels. A procedure that makes use of both visible and near infrared bands has been used to estimate Land Surface Emissivity (LSE), upon which rests the application of the method. This study's focus is to develop a method that processes ERDAS IMAGINE images using band 10 data LANDSAT 8 thermal imagery and band 6 LANDSAT 5 thermal imagery. Findings indicate high LST in built-up areas of the Metropolitan area and low LST in areas with a lot of vegetation cover and water bodies. This study has revealed that NDVI and LST negatively correlate in the area studied. The results show that, with decrease of (LST), there seems to be an increase of vegetation cover (VC). Decrease in vegetation cover, however, seems to be pronounced with increase of (LST). The evidence from this study suggests that, in areas with the highest temperature reaching 49˚C, vegetation is absent. Yet, a dense vegetation cover was found in areas with temperature as low as 12˚C***.

Keywords: LST, NDVI, Al Taif city, Correlation

1. Introduction

During the last decade, many works were devoted to the extraction of land surface Temperature from remote sensing data. Thermal sensors, on board of satellites and planes, offer the possibility of obtaining data about spatially distributed of land surface Temperature. The NOAA-AVHRR, Landsat TM / ETM +, Was In hiding / Aqua Was in hiding MODIS and ASTER supply various scales images for many applications in relation with the earth's surface [1]. Surface temperature is one of many subjects which interested several authors [2] [3] [4] [5] [6] [7] [1].

The extensive request of the surface temperature for the environmental studies and the natural resource activities management made the detection surface temperature more and more an important academic subject [4]. Surface temperature is the key parameter of the earth's physics processes because of its role in the energy between the earth surface and the atmosphere [8]. It is one of the most important parameters in all the earth - atmosphere interactions and this is an important indicator of energy flow between the earth and the atmosphere, as well as being a good indicator of the energy balance on the earth surface [9] [10] [11] [12]. So, the information about the surface temperature (ST) is important for various applications like climatic, hydrological, ecological, agricultural and biogeochemical [2] [4] [5] [13] [14] [15] [16].

The surface temperature, including the sea temperature, is a main geo-biophysics variable to recover from the thermal infrared data (TIR) detection, because most sensor-detected energy in this spectral region is found to be a direct emission from the earth surface [17].

However, the estimated surface temperature from the remote sensing can be useful and can substitute the measures on the earth surface, it is necessary to estimate it with an adequate precision, less than 2°K for energy flows and of the order of 0,3°K for the climate change detection [1].

To solve the problems of surface temperature estimation, it is necessary, to made some intervention such as the calibration of the thermal sensors, the detection of clouds and mainly, atmospheric and emissivity corrections [18].

In this study we will try to detect surface temperature through Landsat images and found the relationship between changing vegetation density and temperature patterns of SW of Taif. To achieve this, the NDVI and land surface temperature (LST) images derived from Landsat TM/OLI-TIRS have been used.

NDVI is mainly used to indicate the vigour of vegetation, its density and its health in any area under study. It is considered the most used vegetation index. NDVI indicator is calculated from red and NIR bands of satellite image data to evaluate if land cover contains green and live vegetation. Rouse et al. [19] are the first who conceived the NDVI index, is founded on light being absorbed and reflected by vegetation. The NDVI is measured by the formula given in equation 3. The NDVI value is comprise between -1 and +1 where -1 correlate with pixel having no vegetation and +1 with pixel with dense vegetation cover. The majority of studies reveal a harmonious correlation between NDVI and vegetation biomass and dynamics in a number of ecosystems globally [20] [21]. In addition, more investigation of NDVI's relationship with climatic variables has supported in accomplishing future predictions possible [22].

Consequently, the NDVI serves as a first favourable tool which can integrate vegetation, climate, ecosystem and environment. It can also be used to undertake studies at larger scales, be they temporal or spatial [23].

The interrelationship between LST and NDVI has been largely reported in the literature. A strong LST and NDVI relationship is proved by Mallick and al. [24] that are using Landsat 7 ETM+ data to found this relationship. Other comparable studies showing a negative correlation between LST and NDVI have been tried [25] [26] [27].

In this piece of research, NDVI is utilized for the sake of deducing LST [28] [29]. It depends on a statistical correlation between the NDVI obtained from the NIR bands and the land surface temperature in the TIR bands [30]. Vegetation quantity determines LST by evapo-transpiration and through a surface to atmosphere latent heat flux. Lower LST is generally characterizing areas with high NDVI [25]. For that reason, the present research has been conducted for the purpose of investigating the spatio-temporal pattern of LST and NDVI in Taif area and study their correlation.

2. Description of Study Area and Data

2.1 Description of Study Area

From geographical point of view, two distinct zones can be identifies in Saudi Arabia: (i) rainy highlands in the western and southwestern regions, and (ii): arid and more arid lands in the interior [31].

The study was undertaken in the Al Taif city that belongs to the largest governorates of the Mecca province (Al Taif governorate) with an area about 3209 km². It is located between latitudes 20°55'19.33"N and 21°46'21.21"N, and longitudes 40°16'34.65"E and 41° 8'20.50"E (**Figure 1**).

Al Taif governorate is characterized by the variations in temperature between its parts, where the average of the temperature in the Najd highland areas in the eastern and northern parts is about 26°c while decreasing at 20°c in the mountainous areas of western and southern parts. It is also characterized by difference in rainfall, where the annual average in desert regions is about 50 mm, and more than 250 mm in mountainous areas.

Al Taif region is marked by diversity in topography, the mountains in the South and in the southernwest which is a part of the Sarawat mountain chains where the dip is very strong towards the Thihama plains and medium to weak towards the East which is characterized by plains and the Najd highland (**Figure 2**).

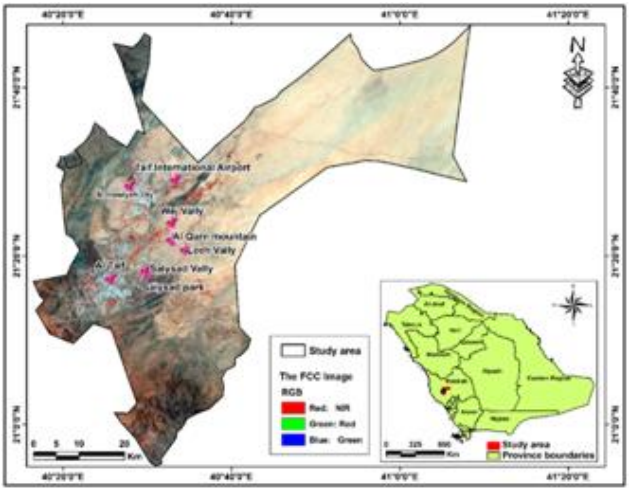

Figure 1: Location map of study area

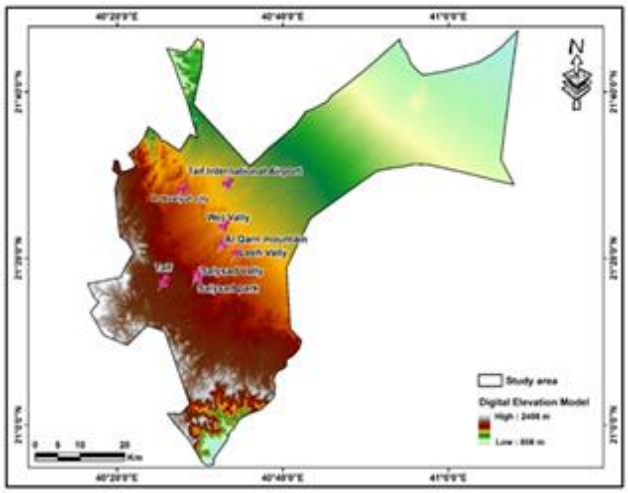

Figure 2: The Digital Elevation Model of Al Taif city

2.2 Data: Satellite Imagery

An image of A Landsat 5 TM, acquired in July 2000 and an image of Landsat 8 OLI_TIRS, acquired in July 2019, formed the primary data source to deriving LST and NDVI in the city of Al Taif and also as a basis to analyze the relationship between these variables. Some metadata are summarized in Table 1. Landsat 5 TM is found to include six reflective bands (visible, near-infrared, and short-wavelength infrared, 30-m spatial resolution), in addition to one band in the TIR region (Band 6) Table 2. The thermal band' native spatial resolution equals 120-m. It is, however, delivered by USGS at 30-m after the resampling of cubic convolution. The Landsat 8 OLI_TIRS sensor has nine reflective bands with 30-m spatial resolution; and two thermal bands (TIRS) capture data with a minimum of 100-meter resolution. However, they are registered to and delivered with the 30-meter OLI data product.

Table 1: Some Landsat metadata and example metadata values

Metadata name	*Landsat5 TM*	*Landsat8/ OLI_TIRS*
Scene ID	LT51690452000195RSA00	LC81690452019183LGN00
sensor	L5_TM	OLI_TIRS
Acquisition Date	2000-07-13	2019-07-02
path	169	169
Row	45	45
Number of bands	7	11
Upper Left Corner Latitude	2501700.000	2512500.000
Upper Left Corner Longitude	545100.000	554100.000
Upper Right Corner Latitude	2501700.000	2512500.000
Upper Right Corner Longitude	777300.000	780900.000
Lower Left Corner Latitude	2291100.000	2280900.000
Lower Left Corner Longitude	545100.000	554100.000
Lower Right Corner Latitude	2291100.000	2280900.000
Lower Right Corner Longitude	777300.000	780900.000

Table 2: The information of Landsat 8 OLI_TIRS and Landsat 5 TM bands (Landsat Project Science Office 2002).

Landsat 8 OLI_TIRS	
Band	*Spatial resolution (m)*
Band 1 Coastal	30 m
Band 2 Blue	30 m
Band 3 Green	30 m
Band 4 Red	30 m
Band 5 NIR	30m
Band 6 SWIR 1	30 m
Band 7 SWIR 2	30 m
Band 8 Pan	15 m
Band 9 Cirrus	30 m
Band 10 TIRS 1	100 m
Band 11 TIRS 2	100 m
Landsat5 TM	
Band	*Spatial resolution (m)*
Band 1 Visible	30 m
Band 2 Visible	30 m
Band 3 Visible	30 m
Band 4 Near-Infrared	30 m
Band 5 Near-Infrared	30m
Band 6 Thermal	120 m
Band 7 Mid-Infrared	30 m

Using USGS website, satellite images of the same region were downloaded at two different dates. The area chosen for the study includes bare soil, water, built-up area and vegetation cover. The nearest neighbor method was used to resample the images. All data reprojection was completed using Universal Transverse Mercator (UTM) coordinate system, with datum WGS84, and with zone 37 N.

3. Methodology

The methodology comprises of one satellite data-based calculations and field-based measurements. For deriving LST and NDVI from satellite data, multi-temporal images (January 2017 and August 2017) acquired in red, near-infrared (NIR) and thermal infrared (TIR) bands of Landsat OLI-TIRS sensors have been used. The digital number (DN) values of pixels in red and NIR bands have been converted to top-of-atmospheric reflectance and later into NDVI. In order to have an estimate of the NDVI temporal variations over the season, images have been density sliced into two classes as defined in the study conducted by Gangopadhyay et al. [32].

1) Non-vegetated Areas: Pixels with NDVI values below 0.1. They include bodies of water, dry river beds, shadow, barren lands, built-up areas (both residential and industrial) and additional no-vegetation areas.
2) Moderate to dense vegetation areas: Pixels with NDVI values above 0.1. They include areas like natural forests and densely vegetative areas.

DN of the thermal bands has been converted to radiant temperature and later into LST for whole of southern west of Al Taif area. Since emissivity, which depends upon surface characteristics, plays an important role in calculation of LST, it has been suitably taken into account to refine the computed LST values. NDVI images have been used to calculate emissivity in this study.

Radiometric calibration, emissivity and atmospheric corrections are needed for the LST satellite-derived TIR measurements [33] [34]. A multiplicity of approaches has been suggested to derive LST from TIR bands, making use of a great number of methods for the purpose of calculating atmospheric effects and emissivity as inputs to the LST computation model [35] [36] [37] [38] [39] [40] [41] [42] [43].

Figure 3: shows the approach suggested to estimate LST. This technique is effective only to process Landsat 8 data. In this study, bands 4 and 5 are used to calculate NDVI. As for, brightness temperature it is estimated using band 10.

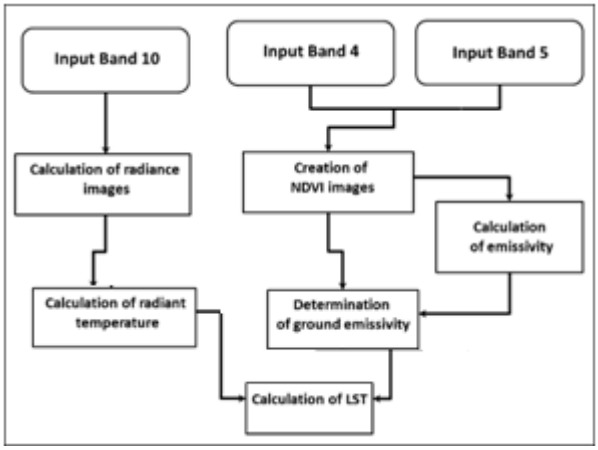

Figure 3: The flow chart of steps to derived LST

The following literature details the steps followed in the work in focus.

a) Calculating radiance images: TM raw digital number (DN) values have been converted to radiance on the basis of Chander et al's formula. [44]:

$$L = (Lmax - Lmin)\, DN + Lmin/DNmax \quad (1)$$

Where L is the spectral radiance received at the sensor; Lmin and Lmax are the minimum and the maximum spectral radiance for the sensor respectively; DNmax is the maximum DN. For TIRS, the formula below is used [45]:

$$L = ML \times DN + AL$$

(2)

Where ML is band specific multiplicative rescaling factor and AL is the band specific additive rescaling factor from the metadata.

b) Radiant temperature calculation: The thermal band-derived radiance images have played a key role in calculating radiant temperature based on the formula below [44]:

$$Tr = K2/ln\ (K1/L + 1)$$

(3)

Where Tr = radiant temperature (in Kelvin); K1 and K2 = pre-launched calibration constants 1 and 2 respectively; L = spectral radiance.

c) NDVI images creation: NDVI hinges on vegetation reflectance and has been calculated using data acquired in Red and NIR band of the Landsat satellite. Bands which were corrected atmospherically have been utilized given that their derived NDVI values are more likely to be representative of the natural surfaces than those derived from DN values. NDVI images have been calculated with reference to Rouse et al's formula. [19]:

$$NDVI = \text{NIR} - \text{Red}/\text{NIR} + \text{Red}$$

(4)

Where Red and NIR are the spectral reflectance of vegetation in the red band and the near infrared band respectively.

d) Emissivity calculation: According to Sobrino et al., [18] An ASTER spectral library included 49 soil spectra. They came up with the expression below, so as to derive LSE from pixels having proportion of both soil and vegetation:

$$\varepsilon = 0.004\ Pv + 0.986$$

(5)

Where Pv = vegetation proportion; NDVI image can be used to derive PV with reference to Carlson and Ripley's equation [46]:

$$Pv = [NDVI - NDVImin/NDVImax - NDVImin]\ 2$$

(6)

Where NDVImax = 0.5 and NDVImin = 0.2. These values (i.e., 0.2 and 0.5) are used for scenes where bare soil and vegetation, respectively, can be found. This equation has been regarded as most suitable in cases of pixels with bare soil and vegetation; this holds true for the area studied.

e) LST calculation: outputs from (3) and (5) have been then considered inputs used to find out the LST, based on the formula below [47]:

$$LST = Tr/1 + (\lambda Tr/\rho)\ \ln\varepsilon$$

(7)

Where λ = central wavelength (in μm) of the Landsat thermal band; ρ = 1.438 * 10-2 m K.

The derived NDVI and LST images served to investigate the spatio-temporal pattern.

4. Results and Discussion

4.1 Spatio-Temporal Analysis of NDVI

To arrive at an approximate calculation of the Spatio-temporal NDVI variations over the Al Taif city, the values of the NDVI were calculated for two images at two different times (2000 and 2019).

Making an analysis of the parameters enumerated in the **Table 3** can account for the fact that there is a decrease in vegetation. The best observation is that the mean and maximum parameters for NDVI show a significant decrease between 2000 and 2019.

Table 3: Statistical data of NDVI

Years	*Minimum*	*Maximum*	*Mean*
2000	-0.12	0.58	0.08
2019	-0.21	0.53	-0.04

Figure 4 show the NDVI for the July 2000 and July 2019. It can be seen that in two images for year 2000 and 2019 the maximum values of the NDVI mark the year 2000. The decrease of the NDVI values at 2019 occur as a response of vegetation regression and urban expansion as seen on **Figure 5a** and **Figure 5b** that show the composite image of the July 2000 and July 2019 respectively.

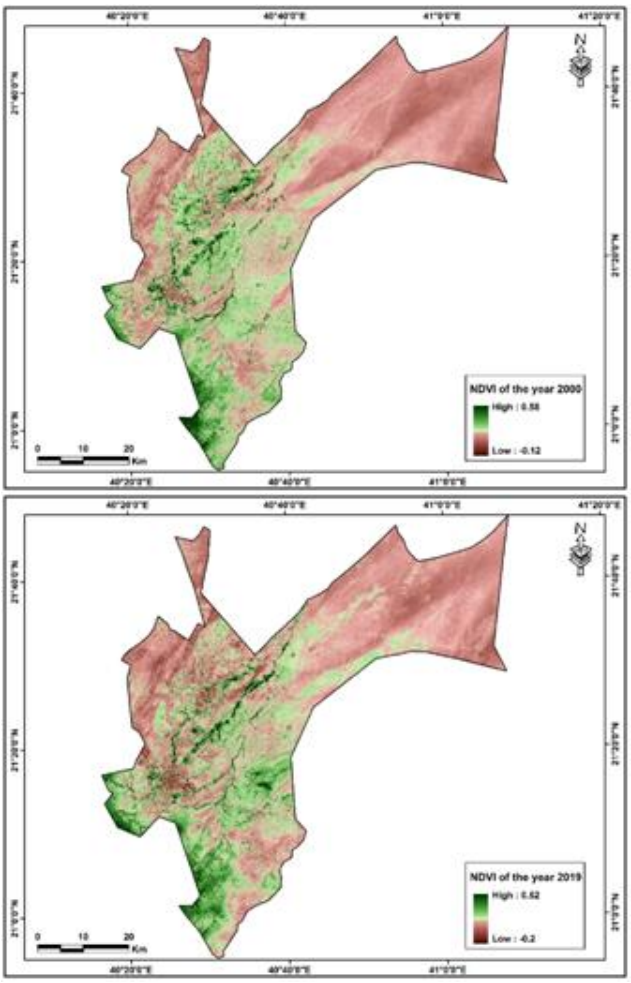

Figure 4: NDVI for the year 2000 and the year 2019

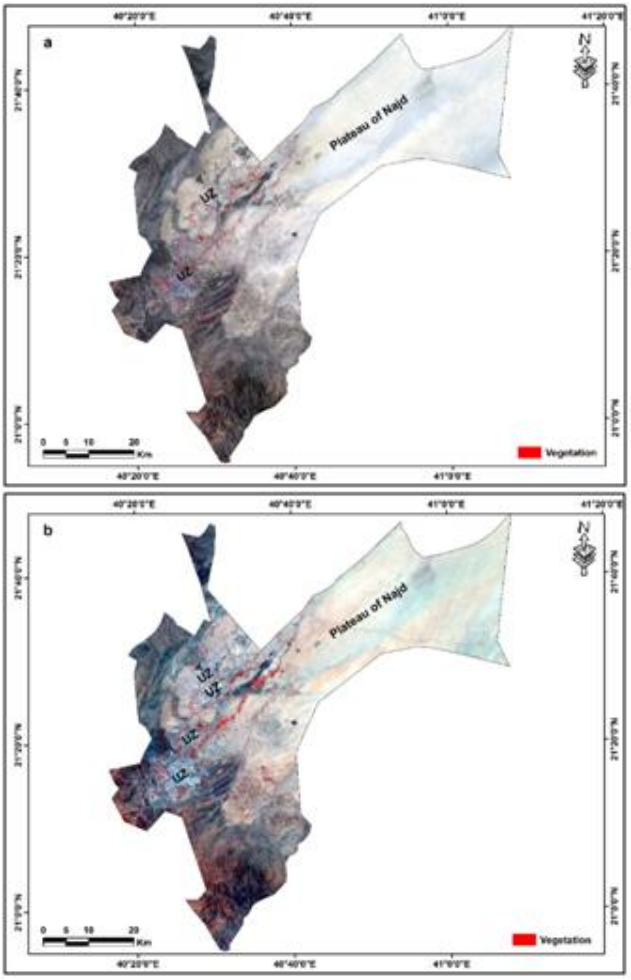

Figure 5: a. The composite image of the year 2000; b. The composite image of the year 2019, UZ: Urban Zone

The values of the highest NDVI (Peak of NDVI) correspond to the Vegetation Area (high and medium altitudes rainforests, cropland and Green Park) where the intensity of green give high reflectance in NIR region and resulting high NDVI values **Figure 6.**

The plant communities having the lowest values of NDVI are located in plateau of Najd (eastern part of Al Taif city), where plant leaves are very scattered (low intensity of green), the minimums values of the NDVI characterize also the urban zone and bare soil **Figure 6.**

4.2 Spatio-Temporal Analysis of LST

The variation of LST has been studied over two periods: 2000 and 2019. **Figure 7** shows the Spatio-temporal distribution of LST for both periods. The minimum values of the LST values mark the year 2000, the maximum of the LST values mark the year 2019 as a response of vegetation regression and urban expansion as seen on Figure 5.

Parameter "mean" is the most important indicator for evaluate changing LST for period 2000-2019. As can be seen in 2000 the value for parameter "mean" was over 38^{o}C. After 19 years there was an increase in this parameter about 5degree **Table 4**. Another important indicator would be the maximum temperature. The difference between 2019 and 2000 is about 4.5 degrees

Table 4: Statistical data of LST

Years	*Minimum*	*Maximum*	*Variations*	*Mean*	*Standard Deviation*
2000	12.36	44.47	32.11	38.39	1.92
2019	25.12	48.81	23.69	42.72	2.36

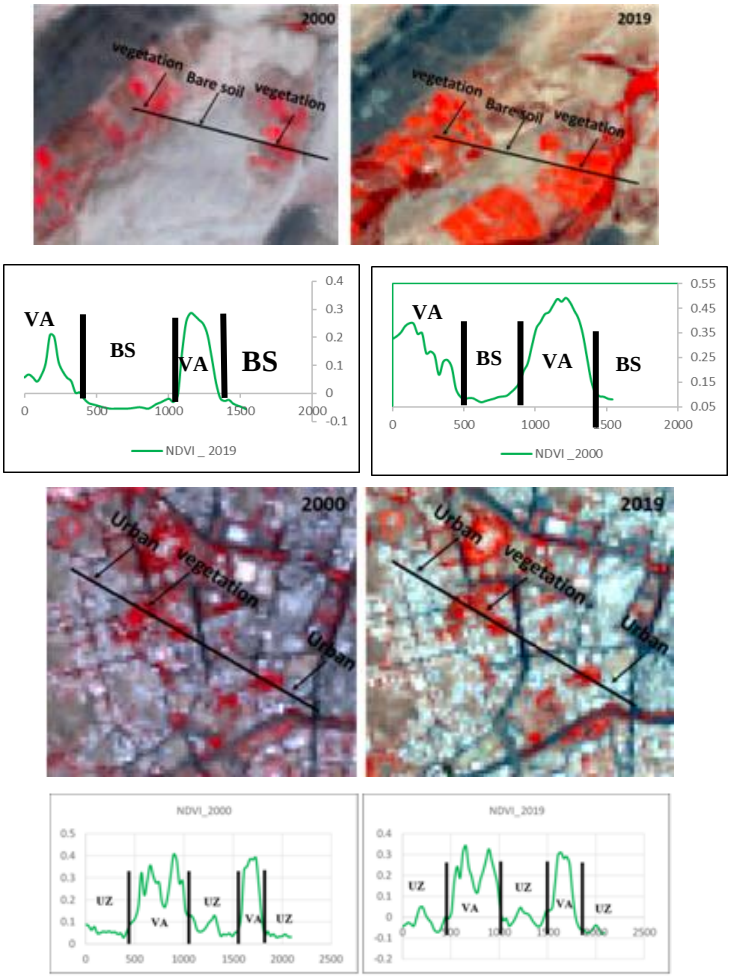

Figure 6: NDVI over some profiles: VA= Vegetation Area; BS= Bare Soil; UZ = Urban Zone

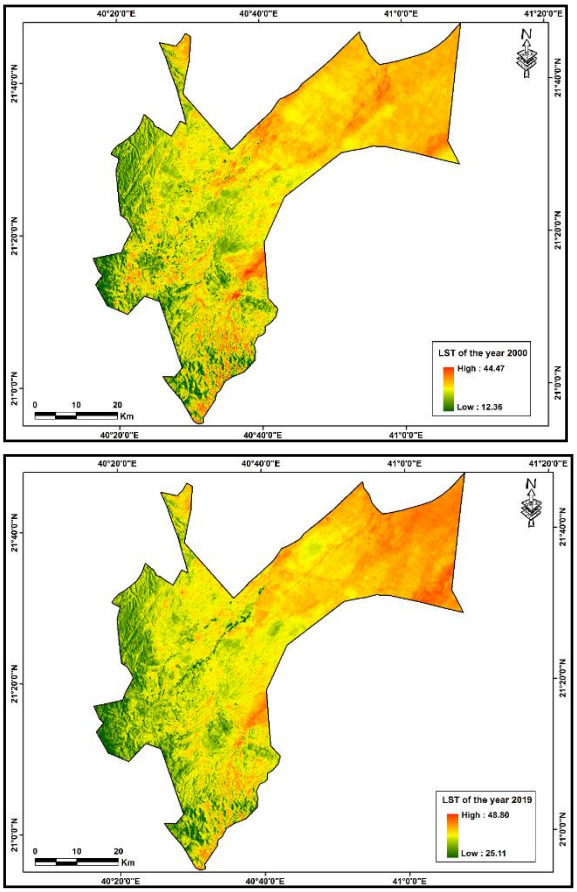

Figure 7: Spatio-temporal variation of LST for the year 2000 and the year 2019

An analysis of LST maps shows the high temperature areas in red and correspond to plateau of Najd, open surfaces or barren hill slopes, built-up areas, bare soil **(Figure 8)** and dried river beds **(Figure 9)**. Whereas the cooler areas are depicted in green and correspond to vegetation area, cropland and water bodies **(Figure 8, Figure 10)**. This is the result of solar energy dissipation by absorbing surrounding heat and leaves' evaporation process.

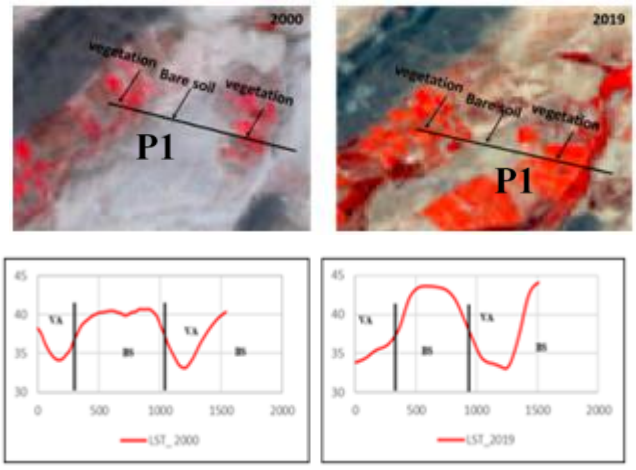

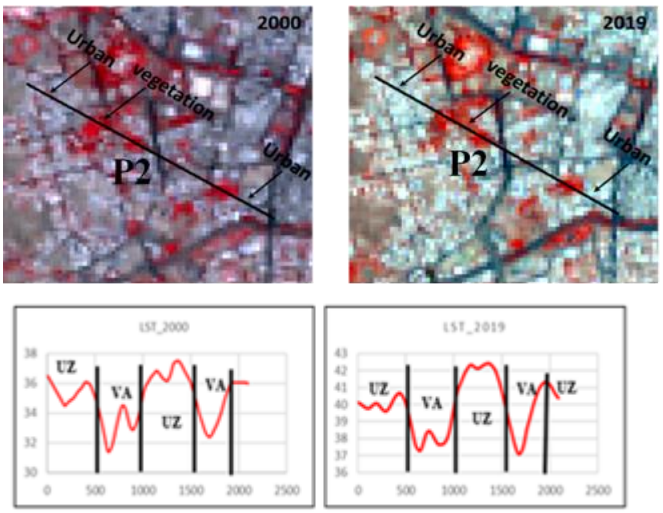

Figure 8: LST over divers profiles: VA= Vegetation Area; UZ = Urban Zone; BS= Bare soil

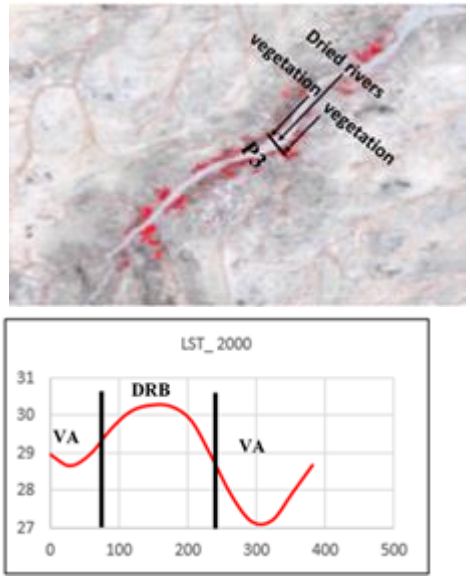

Figure 9: LST over dried river beds and vegetation profile

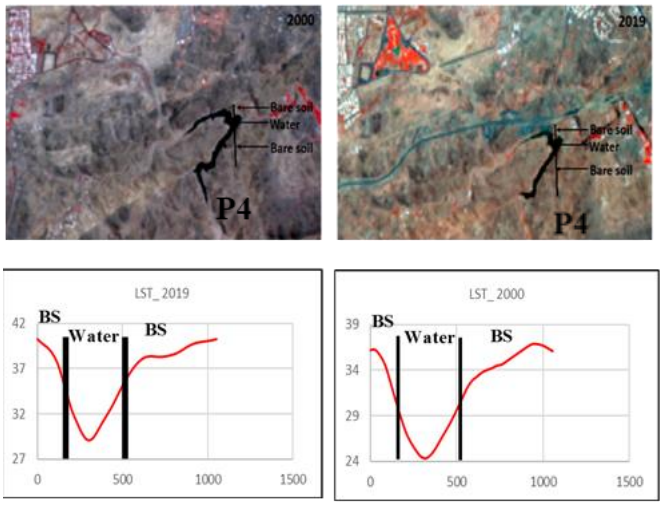

Figure 10: LST over water and bare soil profile: BS= Bare Soil

4.3 Correlation between NDVI and LST

In order to more accurately understand the patterns of NDVI and LST, ERDAS image processing software was used to help simultaneously display the NDVI and LST images of Al Taif city. Figures 4 and Figure 7 informatively and visually depicts the urban thermal environment and vegetation cover spatial patters within Al Taif city. In Al Taif LST image (Figures 4), the urban center LST is higher than that of the suburb. Obviously, higher temperature is associated with urban buildings, where non-porous materials are used, asphalt, metal, and concrete being just a few examples (Lo et al. 1997). In contrast, temperature of, cropland, park, water bodies, and green land is found to be lower. The values, as shown in the NDVI image Figure 7, are the opposite. High values of NDVI are detected within the cropland, park and green land areas; Clearly, the relatively high levels of green biomass has played a key role in this result.

In order for the variance of LST and NDVI to be disclosed in different places at different times, LST and NDVI pixel values are derived on the basis of some profiles (P1, P2, P3) in **(Figure 11, Figure 12** and **Figure 13)**. It is shown in all profiles that the LST peaks are usually located in Urban Zone, Bare Soil and dried rivers beds. The troughs, however, are mostly found in the waters (rivers) and green lands (parks, cropland). The NDVI peaks are found at urban green land, park and cropland. Overall, LST and NDVI are inversely correlated. The LST and NDVI' changing trends are, on the other hand, closely related to Al Taif city's urban sprawl and urban shape.

On the whole, there was an accurate fit in the NDVI-LST regression. While higher R^2 values were observed in P1 and P3 (0.7) at 2000, lower values were observed in P2 at 2000 and in P1 at 2019. The highest R^2 was 0.78 and was observed on P1 at 2000 and the lowest one was 0.52 (P2 at 2000). The relationship between both variables is also demonstrated by Pearson and Spearman correlation coefficients. In all cases, the Pearson indices were higher than -0.7, ranging from 0.72 to 0.88 **(Table 5).**

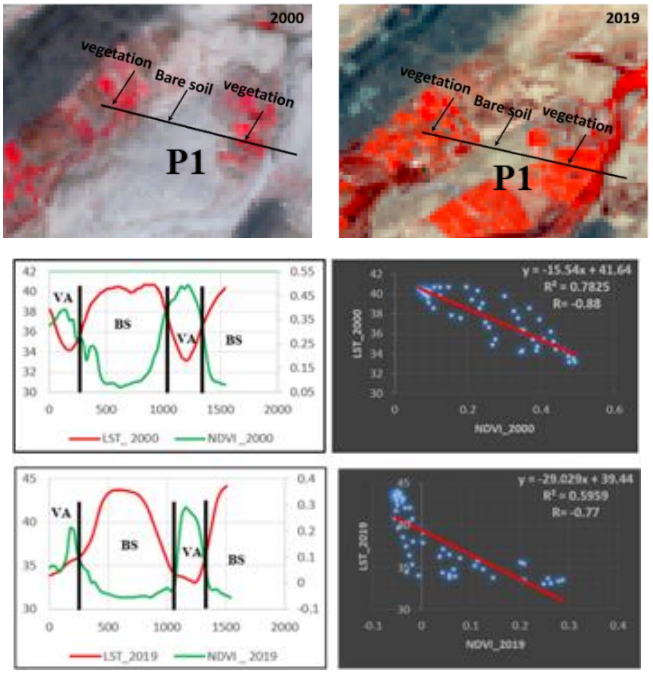

Figure 11: Correlation between NDVI and LST in profile P1(VA= Vegetation Area; BS= Bare Soil)

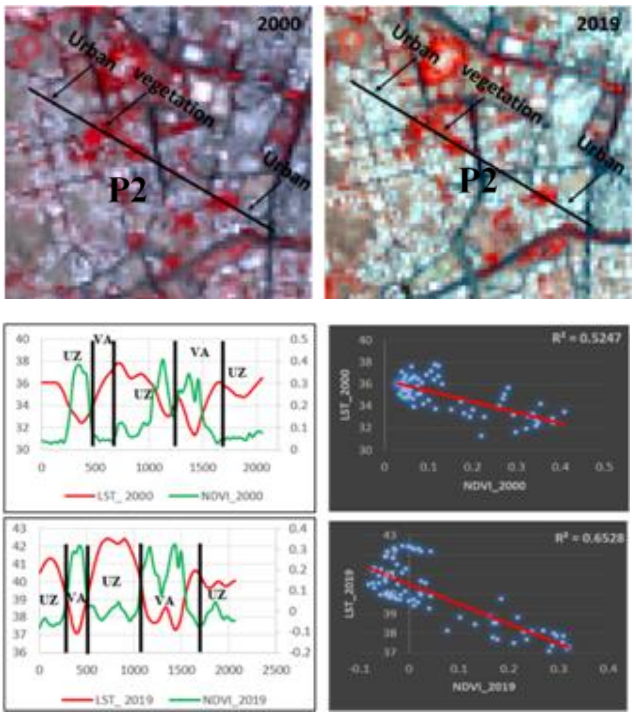

Figure 12: Correlation between NDVI and LST in profile P2 (VA= Vegetation Area; UZ = Urban Zone)

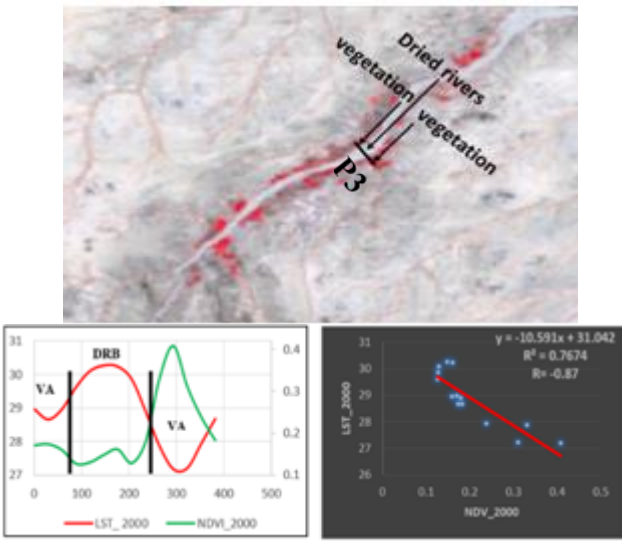

Figure 13: Correlation between NDVI and LST in profile P3 (VA= Vegetation Area; DRB= Dried Rivers Bed)

Table 5: NDVI-LST relationship

Year	*Profiles*	R^2	*R*
2000	P1	0.78	-0.88
	P2	0.52	-0.72
	P3	0.76	-0.87
2019	P1	0.59	-0.77
	P2	0.65	-0.80

5. Conclusion

This study has investigated vegetation the cover and Land Surface Temperature relationship in the city of Al Taif. An integrated approach of remote sensing has been successfully employed for determining NDVI and LST changes using satellite images. Our work has led us to conclude that, in highly vegetated areas, the correlation between the LST trend and the NDVI indicates that the LST trend decreases. The LST trend, however, increases over the desert areas (0 < NDVI < 0.1), showing a more considerable increase of temperature. The decrease in the vegetation is accompanied with the rise in minimum and maximum LST of the area.

References

[1] Zhou, J., LI, J., Zhang, Li., Hu, D., Zhan, W. 2012. Intercomparaison of methods for estimating land surface temperature from Landsat-5 TM image in an arid region with low water vapour in the atmosphere. International Journal of Remote Sensing 33 (8). 2582–2602.

[2] Barton, I.J. 1992. Satellite-derived sea surface temperatures: A comparison between operational, theoretical and experimental algorithms. J. Appl. Meteorol. 31: 432–442.

[3] Lagouarde, J.P., Kerr, Y. H., Brunet, Y. 1995. An experimental study of angular effects on surface temperature for various plant canopies and bare soils, Agric. Forest Meteorol 77: 167–190.

[4] Qin, Z., Karnieli, A. 1999. Progress in remote sensing of land surface temperature and ground emissivity using NOAA-AVHRR data. Inter. J. of Rem. Sens 20: 2367–2393.

[5] Dash, P., Göttsche, F. M., Olesen, F. S., Fischer, H. 2002. Land surface temperature and emissivity estimation from passive sensor data: Theory and practice—current trends. Inter. J. of Remote Sensing 23 (13): 2563−2594.

[6] Schmugge, T., French, A., Ritchie, J.C., Rango, A., Pelgrum, H. 2002. Temperature and emissivity separation from multispectral thermal infrared observations. Remote Sensing of Environment 79: 189–198.

[7] Li, Z.L., Tang, B., Wu, H. 2013. Satellite-derived land surface temperature: Current status and perspectives. Remote Sensing of Environment 131: 14 - 37.

[8] Coll, C. Caselles, V. Galve, J.M. 2005. Ground measurements for the validation of land surface temperatures derived from AATSR and MODIS data. Rem.Sens.Environ. 97: 288-300.

[9] Abdellaoui, A., Becker F., Olory Hevhinger, E. Raffy M. 1983. Influence des conditions de mesure sur l'estimation de l'inertie thermique et de l'évapotranspiration à partir des données Météosat. Proc. du Iième Colloque Intern. Signatures spectrales d'objets en télédétection, Bordeaux (France); 12-16 sept. 1983; éd. INRA; les colloques de l'INRA. INRA. 475-484.

[10] Abdellaoui, A. 1985a. Modélisation de la relation température de l'air – température de surface en vue de l'extension spatiale des modèles d'analyse des paramètres de surface. Proc. Of the 3rd Intern. Colloquium on Spectral Signatures of Objects in Remote Sensing; Les Arcs (France) , ESA SP-247. 171-174.

[11] Abdellaoui, A. 1985b. The fundamental problems for the energy balance study by satellite imagery. Proc.ISLSCP Conference, Roma (Italy).

[12] Abdellaoui, A., Becker F., OloryHechinger, E. 1986. Use of METEOSAT for mapping thermalinertia and evapotranspiration over a limited region of Mali. Journal of Climate andApplied Meteorology 25 (11): 1489-1506.

[13] Caselles, V., Sobrino, J.A. 1989. Determination of frosts in orange groves from NOAA-9 AVHRR data. Remote Sensing of Environment. 29: 135–146.

[14] Vining, R. C., Blad, B.L. 1992. Estimation of sensible heat flux from remotely sensed canopy temperatures, J. Geophys. Res., 97(17), pp: 18951-18954.

[15] Kimura, F., Shimiru, A.P. 1994. Estimation of sensible and latent heat fluxes from soil surface temperature using a linear air land heat transfer model. J. Appl. Meteor 33 (4): 477-489.

[16] Hénon, A. 2008. Températures mesurées, modélisées et observees par télédétection infrarouge dans la canopée urbaine : modélisation aéro-thermo-radiative des flux de chaleur urbains. thèse de doctorat en dynamique des fluides et des transferts, Université de Nantes.

[17] Jimenez Munoz, J.C., Sobrino,J.A. 2008. Split-Window Coefficients for Land Surface Temperature Retrieval from Low-Resolution Thermal Infrared Sensors. IEEE Geosci.Res., Letters 5 (4): 806-809.

[18] Sobrino, J.A., Jiménez-Muñoz, J.C., Paolini, L. 2004. Land surface temperature retrieval fromLANDSAT TM5. Remote Sens. Environ. 90 (4): 434–440.

[19] Rousse, J.W., Haas, R.H., Schell, J.A., and Deering,

D.W. (1973). Monitoring vegetation systems in the great plains with ERTS. In ERTS Symposium, NASA, SP-351, Washington DC, vol. 1, pp. 309-317.
[20] Running, S.W., 1990. Estimating primary productivity by combining remote sensing with ecosystem simulation. In: Remote Sensing of Biosphere Functioning, edited by Hobbs, R.J., Mooney, H.A., Springer-Verlag, Minnesota, pp. 65–86.
[21] Myneni, R.B., Williams, D.L., 1994. On the relationship between FAPAR and NDVI. Remote Sensing of Environment, 49, pp. 200-211.
[22] Gong, D.Y., Shi, P.J., 2003. Northern hemispheric NDVI variations associated with large-scale climate indices in spring. International Journal of Remote Sensing, 24(12), pp. 2559–2566.
[23] Pettorelli, N., Vik, J.O., Mysterud, A., Gaillard, J., Tucker, C.J., Stenseth, N.C., 2005. Using the satellite-derived NDVI to assess ecological responses to environmental change. Trends in Ecology and Evolution, 20 pp. 503–510.
[24] Mallick, J. Kant, Y., Bharat, B.D., 2008. Estimation of land surface temperature over Delhi using Landsat-7 ETM+. Journal of Indian Geophysical Union, 12(3), pp. 131-140.
[25] Yuan, F., Bauer, M.E., 2007. Comparison of impervious surface area and normalized difference vegetation index as indicators of surface urban heat island effects in Landsat imagery. Remote Sensing of Environment, 106(3), pp. 375-386.
[26] Imhoff, M.L., Zhang, P., Wolfe, R.E., Bounoua, L., 2010. Remote sensing of the urban heat island effect across biomes in the continental USA. Remote Sensing of Environment, 114(3) pp. 504–513.
[27] Molnar, G., 2016. Analysis of land surface temperature and NDVI distribution for Budapest using Landsat 7 ETM+ data. Acta Climatologica et Chorologica, 49-50, pp. 49-61.
[28] Valor, E., Caselles, V. 1996. Mapping land surface emissivity from NDVI: application to European, African, and South American areas. Remote Sensing of Environment, 57(3), pp. 167–184.
[29] Sobrino, J.A., Raissouni, N., 2000. Toward remote sensing methods for land cover dynamic monitoring: application to Morocco. International Journal of Remote Sensing, 21(2), pp. 353–366.
[30] Li, Z.-L., Wu, H., Wang, N., Qiu, S., Sobrino, J.A., Wan, Z., et al., 2013. Review article: Land surface emissivity retrieval from satellite data. International Journal of Remote Sensing, 34(9-10), pp. 3084-3127.
[31] Al-Nafie, A. 2008. Phytogeography of Saudi Arabia. Saudi Journal of Biological Sciences 15: 159–176.
[32] Gangopadhyay, P.K., Lahiri-Dutt, K., Saha, K. 2006. Application of remote sensing to identify coalfires in the Raniganj coalbelt, India. International Journal of Applied Earth Observation and Geoinformation, 8(3), pp. 188–195.
[33] Vidal, A., 1991. Atmospheric and emissivity correction of land surface temperature measured from satellite using ground measurements or satellite data. International Journal of Remote Sensing, 12(12), pp. 2449–2460.
[34] Li, Z.-L., Becker, F., 1993. Feasibility of land surface temperature and emissivity determination from AVHRR data. Remote Sensing of Environment, 43(1), pp. 67–85.
[35] Hook, S.J., Gabell, A.R., Green, A.A., Kealy, P.S., 1992. A comparison of techniques for extracting emissivity information from thermal infrared data for geologic studies. Remote Sensing Environment, 42(2), pp. 123–135.
[36] Kerr, Y.H., Lagouarde, J.P., Imbernon, J. 1992. Accurate land surface temperature retrieval from AVHRR data with use of an improved split window algorithm. Remote Sensing of Environment, 41(2-3), pp. 197–209.
[37] Kealy, P.S., Hook, S.J., 1993. Separating temperature and emissivity in thermal infrared multispectral scanner data: Implications for recovering land surface temperatures. IEEE Transactions on Geoscience and Remote Sensing, 31(6), pp. 1155–1164.
[38] Wan, Z., Dozier, J. 1996. A generalized split-window algorithm for retrieving land-surface temperature from space. IEEE Transactions on Geoscience and Remote Sensing, 34(4), pp. 892–905.
[39] Pozo Vazquez, D., Olmo Reyes, F.J., Alados Arboledas, L., 1997. A comparative study of algorithms for estimating land surface temperature from AVHRR data. Remote Sensing of Environment, 62(3), pp. 215–222.
[40] Wan, Z., Li, Z.-L., 1997. A physics-based algorithm for retrieving land-surface emissivity and temperature from EOS/MODIS data. IEEE Transactions on Geoscience and Remote Sensing, 35(4), pp. 980–996.
[41] Gillespie, A.R., Rokugawa, S., Matsunaga, T., Cothern, J.S., Hook, S., Kahle, A.B., 1998. A temperature and emissivity separation algorithm for Advanced Spaceborne Thermal Emission and Reflection Radiometer (ASTER) images. IEEE Transactions on Geoscience and Remote Sensing, 36(4), pp. 1113–1126.
[42] Qin, Z., Karnieli, A., Berliner, P. 2001. A mono-window algorithm for retrieving land surface temperature from Landsat TM data and its application to the Israel-Egypt border region. International Journal of Remote Sensing, 22(18), pp. 3719–3746.
[43] Jiménez-Muñoz, J.C., Sobrino, J.A. 2003. A generalized single-channel method for retrieving land surface temperature from remote sensing data. Journal of Geophysical Research, 108(D22), pp. 4688–4695.
[44] Chander, G., Markham, B.L., Helder, D.L. 2009. Summary of current radiometric calibration coefficients for Landsat MSS, TM, ETM+, and EO-1 ALI sensors. Remote Sensing of Environment, 113(5), pp. 893-903.
[45] USGS, 2014. Using the USGS Landsat 8 product. Retrieved December 11, 2014 from https://landsat.usgs.gov/using-usgs-landsat-8-product
[46] Carlson, T.N., Ripley, D.A. 1997. On the relation between NDVI, fractional vegetation cover, and leaf area index. Remote Sensing of Environment, 62(3), pp. 241–252.
[47] Weng, Q., Lu, D., Schubring, J. 2004. Estimation of land surface temperature–vegetation abundance relationship for urban heat island studies. Remote Sensing of Environment, 89(4), pp. 467-483.